Microstructural Evolution and Corrosion Characteristics of Zn-RE-Mg-Al-Mn Cast Alloys

Ziadoon Tareq Mhawesh MHAWESH, İsmail Hakkı KARA *

Metallurgy and Materials Engineering Department of Engineering Faculty, Karabük University, Karabük,78050, Turkey

https://doi.org/10.5755/j02.ms.42312

Received 22 July 2025; accepted 9 September 2025

In this work, the effects of adding rare earth elements (Nd and Gd) and Mg, Al, and Mn on the microstructure and corrosion characteristics of Zn-based cast alloys were comprehensively studied. Eight different alloy samples were synthesized and analyzed by scanning electron microscopy (SEM), energy-dispersive X-ray spectroscopy (EDX), potentiodynamic polarization (Tafel) experiments, and immersion corrosion tests. Microstructural analysis revealed the presence of dendritic α-Zn phases in the Zn matrix and Nd-rich and Gd-rich intermetallic phases, whose morphology varied depending on the kind and quantity of the additives. The Tafel test values of corrosion potential (*Ecorr*) and current density (Icorr), and the immersion test-derived values of annual corrosion rates (mm/year), were well correlated with the degree of microstructural degradation. Sample Zn + 5 Mg + 0.1 Al + 0.01 Mn + 0.5 Nd + 2.0 Gd, which had the highest corrosion resistance with a higher percentage of Nd and more homogeneous in structure, followed by Sample Zn + 5 Mg + 0.1 Al + 0.01 Mn + 0.1 Nd with the poorest performance. Post-immersion SEM micrographs substantiated the corrosion and electrochemical as well as immersion results, and reiterated that the distribution of intermetallic phases, grain size, and homogeneity of alloying elements are the major parameters governing the corrosion behavior.
Keywords: Zn-based alloys, Nd, Gd, SEM analysis, corrosion resistance.

1. INTRODUCTION

Biodegradable metallic implant materials have drawn more interest in recent years, both in biomedical and as part of green engineering solutions. Zinc (Zn)-based alloys are particularly of significant promise as substitutes for magnesium (Mg) and iron (Fe) alloys for biomedical devices because of their biocompatibility, moderate degradation rate, and adequate mechanical properties [1, 6, 10]. However, the low ductility of Zn-based materials and the challenge of maintaining their degradation rate at the desired level have restricted their use, especially in implantation [10, 13].

In order to overcome such limitations, rigorous research has been focused on the development of multicomponent alloy systems and the incorporation of microalloying additions for enhancing the structural and electrochemical properties of Zn alloys [5, 6, 14]. Zn-Mg alloys have been intensively researched due to the grain-refining property of Mg in the Zn matrix and the enhancement in the mechanical strength [2, 3]. But augmenting the Mg content will trigger the growth of a galvanic cell, hence the likelihood of local corrosion [3, 12]. In order to prevent such an influence and promote the development of passive film, aluminum (Al) addition has been proposed. In Zn-Mg-Al systems, stabilization of the dendritic shape and acquiring more uniform corrosion behavior on the surface is the objective [9, 11].

Recent studies have pointed toward the utility of rare earth (RE) element addition in improving microstructural stability and degradation behavior in Zn-based alloys [5,14]. Among RE elements, neodymium (Nd) and gadolinium (Gd) have been observed to form fine and uniformly dispersed intermetallic phases in Zn alloys, hence enhancing grain boundary strength, inhibiting galvanic corrosion, and leading to a more uniform degradation process [14].

Another study has pointed out the potential of rare earth (RE) microalloying in enhancing the Zn-based biodegradable alloy performance. For instance, hot-extruded Zn–5 wt.% RE alloys showed substantially improved mechanical strength, corrosion resistance, and in vitro and in vivo performances [15]. Nanoscale $MnZn_{13}$ precipitates in Zn–Mn systems have also been shown to promote corrosion resistance and elongation without compromising cytocompatibility and osteogenic activity [16]. A recent comprehensive 2023 research also witnessed that Zn–RE alloys are mechanically stronger and more biocompatible than pure Zn. Additionally, research on Zn–Mg alloys has also proved that the reduction of Mg_2Zn_{11} phase size leads to lower corrosion rates and enhanced bone-forming capacity through controlled Zn/Mg ion release [17]. Collectively, these findings provide a strong incentive for the exploration of Nd and Gd microalloying in Zn–Mg–Al–Mn alloys for a trade-off between mechanical integrity and corrosion behavior for biomedical applications [18].

Nd and Gd were utilized as microalloying additions in the Zn-Mg-Al-based alloys in the current study. The corrosion characteristics of the resulting alloys were investigated in 3.5 % NaCl solution using a combination of potentiodynamic polarization testing and static immersion. This integrated evaluation made it possible to study the role of the composition of alloys on electrochemical properties, revealing the capability of Zn-based biodegradable alloys to

* Corresponding author: İ.H. Kara
E-mail: *ihakkikara@karabuk.edu.tr*

achieve improved surface lifespan and controlled degradation.

2. EXPERIMENTAL STUDIES

2.1. Material preparation

In this study, Zn-Mg-Al-based alloys were synthesized with definite amounts of Nd and Gd by melting and casting at a laboratory scale. High-purity (99.9 %) Zn, Mg, and Al metals and Mg-Gd and Mg-Nd master alloys were melted in an argon protective environment and cast in steel molds to solidify. The alloys were water quenched at room temperature. The solid samples were cut to appropriate sizes, ground, and polished for metallographic analysis and corrosion testing. A heat treatment by homogenization at 350 °C for 4 hours was done. Total of 8 materials were produced and listed in Table 1.

Table 1. Determined chemical compositions of materials

Alloy code	Alloy composition, wt.% additions
1	Zn +5 Mg + 0.1Al + 0.01Mn (base)
2	Base + 0.2 Nd
3	Base + 0.5 Nd
4	Base + 1.0 Nd
5	Base + 0.5 Nd + 0.2 Gd
6	Base + 0.5 Nd + 0.5 Gd
7	Base + 0.5 Nd + 1.0 Gd
8	Base + 0.5 Nd + 2.0 Gd

2.2. Microstructural characterization

The microstructure of the samples was examined on a Scanning Electron Microscope (SEM). Microstructural examination included examination of grain morphology, intermetallic phase distribution, and surface homogeneity. Additionally, the surface chemical composition of the alloy was determined by Energy Dispersive X-ray Spectroscopy (EDX).

2.3. Corrosion tests

2.3.1. Potentiodynamic polarization

Electrochemical corrosion tests were conducted in 3.5 wt.% NaCl solution (≥ 99.5 %) using the technique of potentiodynamic polarization for homogenized samples. An alloy sample was used as the working electrode, platinum as the counter electrode, and Ag/AgCl as the reference electrode in a three-electrode system. Room temperature tests were carried out and measurements obtained under a scan rate of ± 250 mV/s after a 30-minute stabilization period at open-circuit potential. Ecorr and Icorr values were read from the resulting Tafel plots. Coupon size (10 × 10 × 3 mm), solution volume (250 mL per coupon), and number of replicates (n = 3).

2.3.2. Immersion tests

Immersion tests were conducted in accordance with the ASTM G31 standard. Dimensionally standardized and polished specimens were fully immersed in a 3.5 % NaCl solution for predetermined periods (e.g., 24, 48, and 54 hours) to correlate with potentiodynamic corrosion. The products of surface degradation were desorbed using ultrasonic cleaning in distilled water and acetone following immersion, and then the specimens were dried. Corrosion rates (mm/year) were evaluated using the weight loss method.

2.4. Post-immersion surface analysis

After immersion tests, the corrosion surfaces were analyzed again using SEM. The analysis focused on the morphological features of corrosion products, crack growth, pitting microstructures, and degradation characteristics of the alloys as a whole. EDX analysis was also performed to examine the elemental features of corrosion products to determine how the NaCl solution had influenced the alloy surfaces. ImageJ software was used to porosity distribution.

3. RESULTS AND DISCUSSION

3.1. Microstructural properties

The composition and microstructure studies of Zn-Mg-Al-Mn alloys micro alloyed with Nd and Gd micro addition elements revealed strong correlations between alloy composition and achieved structural properties (see Fig. 1 and Table 2). SEM-EDX analysis confirmed that zinc was the major phase in all samples and possessed a maximum of 95.58 wt.% concentration in Sample 5. This means Sample 5 best represents pure Zn in matrix composition, which would be useful to ensure biocompatibility. On the other hand, Sample 7 contained the lowest amount of Zn (90.33 wt.%), corresponding to the highest number of secondary phases due to the highest total content of alloying elements.

Table 2. Average elemental content of samples obtained by EDX, wt.%

Sample	Zn	Mg	Al	Mn	Nd	Gd
1	91.49	7.92	0.12	0.47	–	–
2	91.18	2.56	0.48	0.18	4.48	–
3	94.52	0.34	1.26	0.80	3.08	–
4	92.82	1.40	0.45	1.61	3.72	–
5	95.58	0.28	0.13	1.47	0.35	2.19
6	92.50	2.51	0.37	0.24	0.58	3.79
7	90.33	4.41	0.37	1.09	1.96	1.83
8	92.36	0.36	1.34	1.83	3.07	1.04

Magnesium, possessing strengthening and grain-refining in Zn matrices, was also present at the maximum concentration in Sample 1 (7.92 wt.%) to form a eutectic Zn-Mg structure. It also possessed the most uniform and uncomplicated microstructure. On the other hand, although Sample 7 had a moderate Mg composition (4.41 wt.%), it is nevertheless sufficient to enhance mechanical strength. Low Mg content samples (e.g., Sample 3 and Sample 8) showed less complicated and more uniform microstructures, which implies a trade-off between the simplicity of microstructure and improvement in mechanics (see Table 2).

The addition of neodymium played a significant role in grain refinement and the formation of intermetallic phases. Notably, Sample 2 with a nominal increase of 0.2 wt.% Nd exhibited an unusually high Nd concentration locally (4.48 wt.%), and this needs to be attributed to microsegregation. Sample 4 and Sample 8 also exhibited high Nd contents (3.72 and 3.07 wt.%, respectively), but with a preference to fine and homogeneous grains.

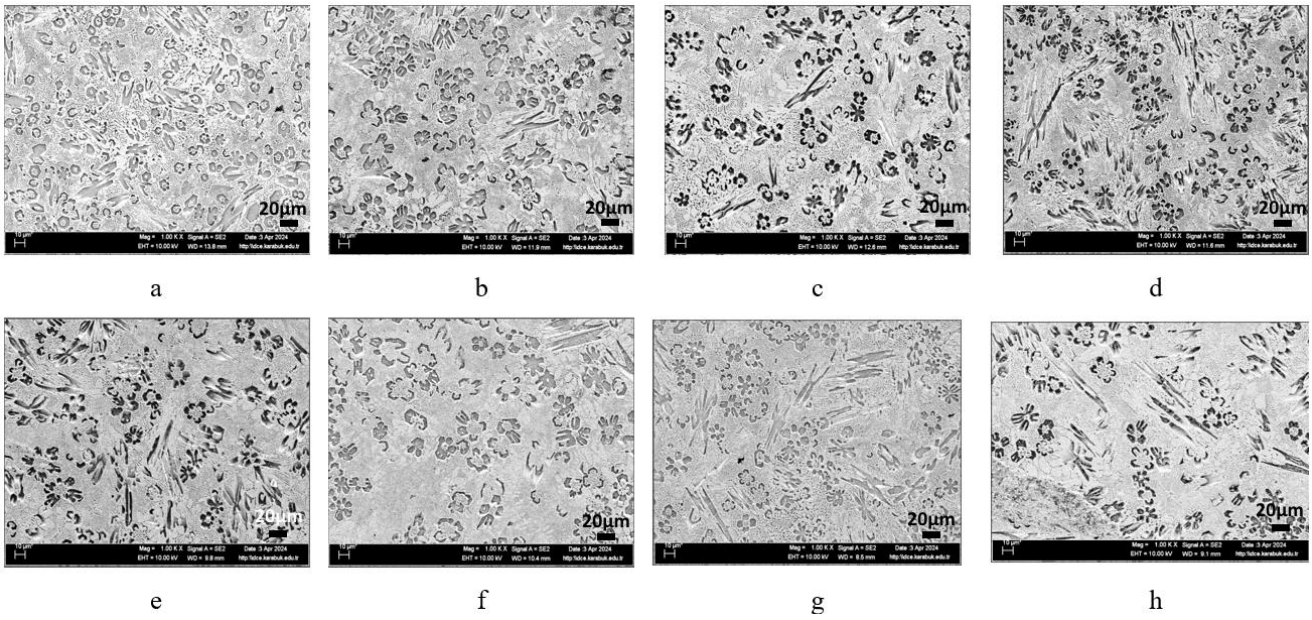

Fig. 1. SEM images of as-cast materials of a – 1; b – 2; c – 3; d – 4; e – 5; f – 6; g – 7; h – 8

Out of these, Sample 4 had the highest fine and uniform microstructure that can play a significant role in improving mechanical properties. In contrast, Sample 5 with the lowest Nd content (0.35 wt.%) had a coarser grain and lower phase complexity, which reflects the negligible impact of rare earth modification. This suggests that there is a threshold content of RE to induce the favorable microstructural refinement mechanisms (see Table 2). The gadolinium effect was most significant in Sample 6, with the highest content of Gd (3.79 wt.%) and clear segregation and phase clustering evidence.

Microstructural features of this kind correspond to increased brittleness and potential mechanical instability, especially in cyclic loading or dynamic physiological conditions. Sample 5, Sample 6, and Sample 7, with various ratios of Gd content, all exhibited intermetallic phase clustering, highlighting the importance of regulating Gd composition to avoid a negative effect on ductility (see Table 2).

Based on overall performance, Sample 4 would be the ideal candidate for high-mechanical-strength applications due to its uniform, dense, and fine-grained microstructure. Similarly, Sample 7, which finds a balance between moderate levels of Mg, Nd, and Gd, is also an ideal candidate for strength-based applications, though with a multi-phase structure.

Sample 6 and Sample 8, however, might be more desirable where there is a need for high hardness and resistance to thermal conditions, presumably owing to their multi-phase network structure, but this may be at the cost of reduced ductility. In corrosion-resistant use, Sample 1 and Sample 2 are useful owing to their reasonably high Mn and Mg contents, which stabilize passive films and reduce local corrosion. Conversely, Sample 3 and Sample 5 have good control of intermetallic phases and therefore are suited to applications where both corrosion resistance and structural homogeneity.

3.2. Corrosion performance

Sample 6 demonstrates the lowest corrosion rate (ca. 0.127 mpy), indicative of superior corrosion resistance. Sample 8 registers the highest corrosion rate (11.33 mpy) and thus is the least corrosion-resistant in the group. Sample 1 – Sample 5 and Sample 7 have the relatively moderate corrosion rates of 1.3 to 4.8 mpy. As the Nd content increases, outstanding corrosion resistance is achieved in some samples, namely Sample 6 (see Fig. 2). Sample 6 has the lowest corrosion rate (approximately 0.127 mpy), indicating better corrosion resistance. This is as compared to Sample 8, which has the highest corrosion rate (11.33 mpy) and is the least corrosion-resistant of all the samples.

Table 3. Comparison of Tafel extrapolation results for Zn-Mg-Al-Mn alloys with Nd and Gd additions in 3.5 % NaCl

Sample code	*Ecorr*, V	*Icorr*, A/cm²	Anodic slope, mV/dec	Cathodic slope, mV/dec	*Icorr* a, A/cm²	*Icorr* c, A/cm²
1	-0.968	-4.2×10^{-5}	1611.3	-2624.6	-0.0001×10^{-5}	-6.7×10^{-5}
2	-0.879	~0,0001	538.5	-9545.5	1.0×10^{-6}	~0.0001
3	-0.886	1.0×10^{-5}	311.0	-9892.5	1.0×10^{-6}	1.0×10^{-5}
4	-0.752	1.0×10^{-5}	1291.7	-12243.6	~0.0001	1.1×10^{-5}
5	-0.936	1.0×10^{-5}	-1294.7	-16666.7	-3.0×10^{-6}	9.0×10^{-6}
6	-1.004	-2.4×10^{-5}	5540.2	-827.7	-2.0×10^{-6}	-1.67×10^{-4}
7	-0.936	6.0×10^{-6}	2960.2	-9583.3	0.0001	7.0×10^{-6}
8	-0.745	-9.0×10^{-6}	-155.4	-605.3	2.7×10^{-5}	1.0×10^{-6}

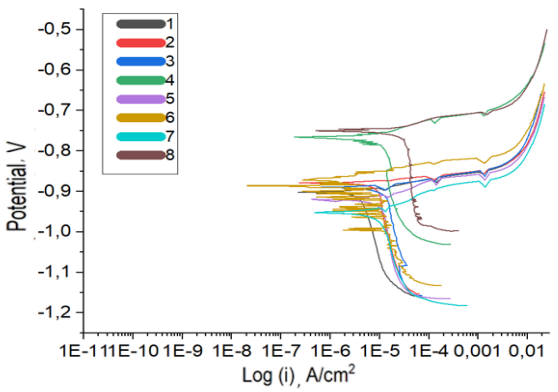

Fig. 2. Tafel plots of samples

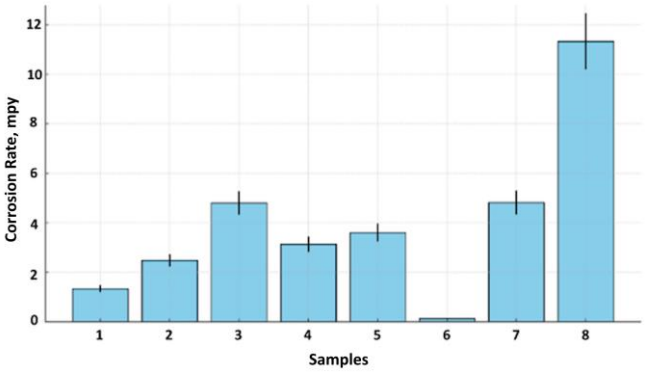

Fig. 3. Corrosion rate of samples obtained by Tafel plots

Sample 1 – Sample 5 and Sample 7 have moderate corrosion rates between 1.3 and 4.8 mpy. On increasing the content of Nd, there is a remarkable improvement in corrosion resistance in certain samples, particularly in Sample 6 (see Table 3).

The corrosion behavior of the Zn-Mg-Al-based alloys, as determined by both potentiodynamic polarization (Tafel extrapolation) and long-term immersion exposure, was notably dissimilar in between the various alloy compositions. This is a direct reflection of the influence of the Nd and Gd microalloying elements on both electrochemical reactivity and structural integrity (see Fig. 2).

Based on the Tafel extrapolation measurements, the corrosion potential (*Ecorr*) and corrosion current density (*Icorr*) were notably dissimilar for the different samples. The lowest value of *Ecorr* was recorded for Sample 6 (−1.004 V), which is typical of highly anodic behavior and poor corrosion resistance. Conversely, the highest positive value of *Ecorr* (−0.745 V) was found in Sample 8, indicating a more passive surface and improved corrosion protection. In the case of *Icorr*, the highest value (4.2×10^{-5} A/cm²) was recorded in Sample 1, which is representative of an elevated dissolution rate and poor corrosion performance. In contrast, Sample 2 displayed a near-zero *Icorr* value, indicating passivity, possibly due to spontaneous film formation or test conditions restrictions on electrochemical activity [3,6].

Though cathodic Tafel slopes were higher than 10,000 for some samples (Sample 4 and Sample 5), indicating fast cathodic reactions, the adverse anodic slope values in some alloys (Sample 5) could be suggestive of experimental fluctuations or instability of data while fitting the curves. Nevertheless, Sample 8 exhibited the best corrosion performance overall among Tafel measurement because it had low *Icorr* and nobler *Ecorr* values (see Fig. 2 and Fig. 3). Simultaneously with immersion tests, time-dependent degradation behavior was examined by studying test results. Sample 4 of immersed samples experienced the greatest total weight loss and highest corrosion rate (0.3884 mm/year), representing the worst corrosion resistance and sensitivity to long-term degradation. At the opposite extreme, Sample 8 possessed the lowest corrosion rate (0.3469 mm/year) and the lowest percentage weight loss and thus proved to be the most resistant alloy against corrosion under static immersion.

While Sample 6 had a higher rate of dissolution on the second day, its general corrosion rate was moderate, indicating a possible stabilization as time passed [5].

Compared to the two test methods, striking observations emerged. Sample 4, which had intermediate corrosion activity in the Tafel test (*Icorr* = 1.0×10^{-5} A/cm²), had the highest long-term corrosion rate in immersion testing, indicating the lack of an inhibiting film and continuous degradation as a function of time. Sample 6, although with a quite high *Icorr* value (2.4×10^{-5} A/cm²), exhibited more stable and less rapid corrosion on immersion, possibly due to the formation of a semi-protective corrosion layer after initial surface activation. Sample 8 was consistently found to have the lowest corrosion rates by either test procedure, indicative of an intrinsically stable and protective alloy structure with outstanding resistance to both time-independent and time-dependent corrosion processes [14]. Following homogenization heat treatment, SEM examination revealed significant differences between the samples (see Fig. 4).

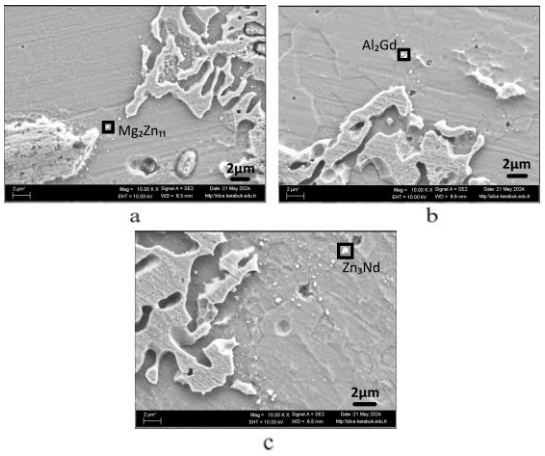

Fig. 4. SEM images of samples after homogenization heat treatment: a – Sample 4; b – Sample 6; c – Sample 8

Sample 8 exhibited the most uniform structure, with well-developed grains and minimal phase contrast. Most intermetallic phases seemed to have dissolved, and the surface was smooth without visible corrosion residues, making it the most responsive to the homogenization treatment. Overall, the heat treatment significantly improved the microstructural uniformity and surface integrity of Sample 6 and Sample 8, potentially enhancing both mechanical and corrosion resistance. In contrast, Sample 4 was the least responsive, possibly due to its

composition, which suggests it may require a longer duration or an adjusted temperature profile for optimal results.

This way, the agreement between SEM observations and corrosion testing results highlights the importance of combining both short-term electrochemical techniques and long-term immersion tests to accurately describe the corrosion behavior of biodegradable alloys. While Tafel analysis helps understand initial dissolution tendencies, immersion tests capture cumulative degradation and protective layer formation effects. Sample 8 was the most resistant to corrosion among the alloys, whereas Sample 4 showed the poorest performance in all aspects. Sample 6 displayed an intermediate profile with some potential for corrosion control through microstructural optimization and surface treatment [12]. RE elements have been found to promote microstructural refinement and intermetallic phase development, serve as effective grain boundary pinning agents, and reinforce the alloy matrix [14, 17]. In particular, Du et al.'s work [14] demonstrated that the addition of even small amounts of RE (Sc, Y, La–Nd, Sm–Lu) significantly altered Zn-based alloys' corrosion behavior and biocompatibility by influencing passive film stability and inhibiting local corrosion. Similarly, Tong et al. [17] showed that hot-extruded Zn–5RE alloys (Y, Ho, Er) exhibited improved mechanical properties and consistent degradation owing to the synergistic effects of solid solution strengthening and RE-containing intermetallics.

Sample 4 had moderate-to-high corrosion activity from its Icorr value (1.0×10^{-5} A/cm²) but also displayed one of the highest mass loss rates in the immersion test (0.3884 mm/year). This anomaly can be due to microstructural porosity or localized galvanic effects that promote degradation under static conditions, even with average electrochemical reactivity [8].

Sample 6 also showed a greater corrosion tendency electrochemically ($Icorr = 2.4 \times 10^{-5}$ A/cm²), indicating susceptibility to anodic reactions upon dynamic potential scanning. The immersion test, however, showed a comparatively moderate corrosion rate (0.3581 mm/year), which reveals that the alloy may develop a semi-stable passive layer upon long exposure, which would provide some resistance to uniform degradation [7].

Sample 8 showed the best corrosion performance consistently in both techniques: an Icorr of 9.0×10^{-6} A/cm² and a low mass loss rate of 0.3469 mm/year. This suggests that its microstructural characteristics – possibly enhanced by optimized Nd and Gd additions – enable it to exhibit better corrosion resistance, likely through a refined grain structure and reduced galvanic coupling [5].

Table 4. Immersion corrosion resulting from samples

Sample	Total loss, g	Corrosion rate, mg/cm²/day	Corrosion penetration, mm/year	Corr. rate, mpy	Percentage loss, %
4	0.0101	0.7597	0.3884	15.29	0.22%
6	0.0093	0.7004	0.3581	14.10	0.21%
8	0.0094	0.6786	0.3469	13.66	0.19%

Sample 4 displayed the highest total mass loss and corrosion rate, with a penetration value of 0.3884 mm/year, indicating a relatively aggressive degradation behavior (see Table 4). Despite its promising mechanical structure, its corrosion resistance under immersion conditions is comparatively lower, possibly due to micro-galvanic coupling or insufficient passive film formation [4 – 6].

Sample 6 had a marginally lesser mass loss and corrosion rate compared to Sample 4, with a similar corrosion depth. Corrosion percentage loss of 0.2052 % indicates a moderate yet uniform degradation profile and hence is a balanced choice where both strength and corrosion behavior are taken into account.

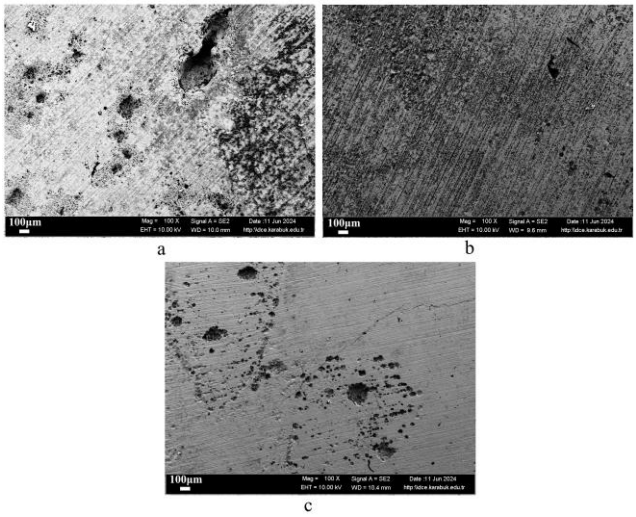

Fig. 5. SEM images of samples after corrosion heat treatment: a – Sample 4; b – Sample 6; c – Sample 8

Sample 8 performed the best in corrosion resistance with the lowest corrosion rate (0.6786 mg/cm²/day) and the lowest mass loss. The percentage weight loss of 0.1881 % assures that this alloy possesses better stability under immersion conditions, which may be due to balanced Nd–Gd alloying and refined microstructure.

Post-immersion SEM analysis also supported these findings. Sample 4 had extreme surface deterioration with intense pitting, grain boundary separation, and extensive surface irregularities, as expected for its low corrosion resistance and excessive material loss. Sample 6, although showing some linear corrosion marks and localized attack, had a relatively smooth surface with uncompromised grain morphology, as expected for stabilization shown in immersion testing. Sample 8 also possessed the most preserved surface, lower pitting, and intact microstructural integrity, and it exhibited a good correlation with its excellent corrosion response in electrochemical as well as immersion-type testing (see Fig. 5). Recent advances also continue to support the role of precipitation phenomena and nanoscale phases in alloy performance control. For example, Dong et al. [16] stressed that the nanoscale precipitates in Zn–Mn alloys not only hardened the alloys but also improved corrosion resistance and cellular response, which are comparable to the effects caused by RE-based precipitates in our system. Besides, mechanical processing routes such as rotary swaging were reported to have a strong grain refinement and enhancement in strength of Zn–Mg alloys [15], further establishing the importance of control of microstructure in determining mechanical and corrosion properties.

3.3. SEM after immersion testing

SEM observations indicated that there were clear differences among the samples' corrosion behavior. Sample 4 was subjected to severe corrosion damage with heavy pitting, strong grain boundary degradation, and surface irregularities, showing high material loss and poor structural resistance (see Fig. 6).

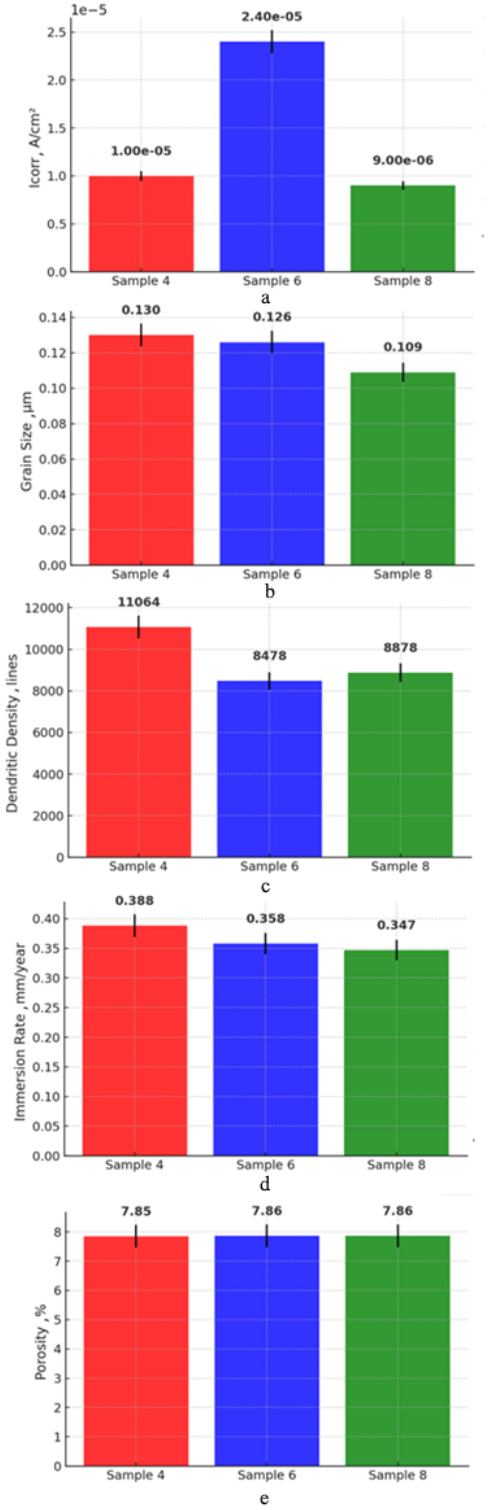

Fig. 6. Relationship between microstructure and corrosion: a – i_{corr}; b – grain size; c – dentritic density; d – immersion rate; e – porosity % .

Sample 6 presented a more homogeneous surface with restricted linear corrosion traces and maintained its granular texture, which suggests a controlled but moderately stabilized corrosion behavior. Sample 8 was distinguished by the least surface deformation, minor pitting, and a highly preserved microstructure, indicating the best corrosion resistance under microscopic examination, as well as in agreement with immersion test findings. These post-immersion SEM findings are in very good agreement with both potentiodynamic (Tafel) and immersion test results, since the degree of microstructural degradation is consistent with the corrosion tendency determined in electrochemical tests (see Table 5).

Table 5. Comparison of potentiodynamic and immersion corrosion results

Sample	*Icorr*, A/cm²	Tafel-based corrosion	Immersion rate, mm/year	Immersion-based corrosion
4	1.0×10^{-5}	Moderate-to-high corrosion	0.3884	Among the highest corrosion rates
6	2.4×10^{-5}	High corrosion tendency	0.3581	Relatively low but steady dissolution
8	9.0×10^{-6}	Low-to-moderate corrosion	0.3469	Lowest corrosion – best performing alloy

To be specific, Sample 4 performed poorly with a moderately high *Icorr* value (1.0×10^{-5} A/cm²) and the highest corrosion rate (0.3884 mm/year) in the immersion test, which is in good agreement with the heavily pitted and degraded SEM surface. Sample 6, while having a relatively high Icorr (2.4×10^{-5} A/cm²) in the Tafel test, showed a more stable behavior in immersion (0.3581 mm/year), and its mild pitting and preserved surface in SEM images validate this stabilization. Sample 8 performed the best with a low-to-moderate *Icorr* value (9.0×10^{-6} A/cm²) and the lowest corrosion rate (0.3469 mm/year), while SEM imaging showed an intact surface and minimal pitting, corroborating its superior corrosion resistance. In summary, the SEM findings strongly corroborate the electrochemical trends in potentiodynamic and immersion testing, offering an accurate representation of the corrosion behavior of each sample. Sample 8 had the best corrosion resistance with the lowest Icorr and immersion rate, which correlates with its refined grain size (0.109 µm), moderate dendritic structure, and low porosity – factors that tend to minimize microgalvanic activity and promote passive film stability. On the contrary, Sample 4, even with similar porosity, performed the worst in corrosion, mainly because of its high dendritic density (11,064 lines), which tends to promote microgalvanic coupling and heighten electrochemical activity at the interfaces. Sample 6 was a contradictory case: even though homogenization decreased its dendritic complexity, it nevertheless had the highest Icorr, which means that corrosion behavior can also rely on other factors such as phase distribution or localized galvanic effects aside from porosity. All in all, the comparison affirms that lower grain size and lower dendritic complexity greatly improve

corrosion resistance, with Sample 8 being the most corrosion-resistant microstructure.

Sample 4 shows the most intense localized attack, with the largest pit number and overall damaged area, in support of its poor corrosion resistance and microstructural complexity. Sample 6, although improved by homogenization, continues to manifest considerable general corrosion, possibly due to residual phase or chemical inhomogeneities. Conversely, Sample 8 demonstrates the lowest pit number and most even pit distribution, in support of its being the most corrosion-resistant sample, as shown through the foregoing electrochemical and structural evaluations. This emphasizes the high correlation between refined, homogeneous microstructure and enhanced corrosion performance [8, 9]. The electrochemical processes were unraveled in the frame of saline environments. RE additions influence the balance between anodic dissolution of Zn and cathodic oxygen reduction/hydrogen evolution and consequently regulate the total degradation kinetics. Refining the grain structure and the presence of RE-rich phases contribute to more electrochemical activity homogeneity, preventing localized pitting and the establishment of a more controlled degradation profile [14, 17]. All these findings collectively confirm mechanistic basis for increased corrosion resistance and biocompatibility achieved through introducing RE elements in Zn-based biodegradable alloys.

4. CONCLUSIONS

In the present research, eight Zn-based cast alloys with different additions of Mg, Al, Mn, and rare earth metals (Nd, Gd) were manufactured. Their microstructural characteristics, chemical compositions, and corrosion resistance were extensively examined. SEM and EDX data indicated that all specimens were mostly composed of the α-Zn phase. Mg, Nd, and Gd additions were found to strongly affect phase formation, grain size, and microstructure uniformity. High Mg content (particularly in Sample 1 and Sample 7) resulted in the development of Zn–Mg eutectic structures, whereas Nd and Gd favored the formation of intermetallic phases and segregation.

Potentiodynamic (Tafel) tests revealed that sample 1 presented the highest corrosion tendency (*Icorr*: 4.2×10^{-5} A/cm²), whereas Sample 2 presented the lowest, with passive behavior. Sample 8 presented the most positive corrosion potential (*Ecorr*), showing the best electrochemical corrosion resistance. In immersion tests, after three days, Sample 4 presented the greatest material loss (0.3884 mm/year), whereas Sample 8 presented the lowest (0.3469 mm/year). Post-immersion SEM analysis corroborated these results: Sample 4 presented severe pitting and surface degradation, whereas Sample 8 presented slight surface damage and a homogeneous structure.

Acknowledgements

The authors gratefully acknowledge the financial support from the Scientific Research Projects Coordination Unit of Karabük University under Project No. KBÜBAP-24-DS-038.

REFERENCES

1. **Zhang, S., Zhang, X., Zhao, C., Li, J., Song, Y., Xie, C., Yu, G., Zhang, Y., He, Y., Jiang, Y., Bian, Y.** Research on an Mg–Zn Alloy as a Degradable Biomaterial *Acta Biomaterialia* 6 (2) 2010: pp. 626 – 640. https://doi.org/10.1016/j.actbio.2009.06.028
2. **Yao, C., Wang, Z., Tay, S.L., Zhu, T., Gao**, **W.** Effects of Mg on Microstructure and Corrosion Properties of Zn–Mg Alloy *Journal of Alloys and Compounds* 602 2014: pp. 101 – 107. https://doi.org/10.1016/j.jallcom.2014.02.048
3. **Prosek, T., Nazarov, A., Bexell, U., Thierry, D., Serak, J.** Corrosion Mechanism of Model Zinc–Magnesium Alloys in Atmospheric Conditions *Corrosion Science* 50 (8) 2008: pp. 2216 – 2231. https://doi.org/10.1016/j.corsci.2008.05.018
4. **Koll, T., Ullrich, K., Faderl, J., Hagler, J., Schuhmacher, B., Spalek, A.** Properties and Potential Applications of Novel ZnMg Alloy Coatings on Steel Sheet *Metallurgical Research & Technology* 101 (7 – 8) 2004: pp. 543 – 550. https://doi.org/10.1051/metal:2004143
5. **Maruf, M.A., Noor-A-Alam, M., Haider, W., Shabib, I.** Enhancing Controlled and Uniform Degradation of Fe by Incorporating Mg and Zn Aimed for Bio-Degradable Material Applications *Materials Chemistry and Physics* 285 2022: pp. 126171. https://doi.org/10.1016/j.matchemphys.2022.126171
6. **Kalhor, A., Rodak, K., Tkocz, M., Myalska-Głowacka, H., Chmiela, B., Wątroba, M., Boczkal, S., Junak, G.** Microstructure, Mechanical Properties, and Corrosion Behavior of a Biodegradable Zn–1.7Mg–1Ca Alloy Processed by Kobo Extrusion *Materials Science and Engineering: A* 887 2023: pp. 145771. https://doi.org/10.1016/j.msea.2023.145771
7. **Bowen, P.K., Seitz, J.M., Guillory, R.J., Braykovich, J.P., Zhao, S., Goldman, J., Drelich, J.W.** Evaluation of Wrought Zn–Al Alloys (1, 3, and 5 Wt% Al) through Mechanical and in Vivo Testing for Stent Applications *Journal of Biomedical Materials Research Part B: Applied Biomaterials* 106 (1) 2018: pp. 245 – 258. https://doi.org/10.1002/jbm.b.33824
8. **Panossian, Z., Mariaca, L., Morcillo, M., Flores, S., Rocha, J., Peña, J.J. Simancas, J.** Steel Cathodic Protection Afforded by Zinc, Aluminium and Zinc/Aluminium Alloy Coatings in The Atmosphere *Surface and Coatings Technology* 190 (2 – 3) 2005: pp. 244 – 248. https://doi.org/10.1016/j.surfcoat.2004.03.023
9. **Hammam, R.E., Abdel-Gawad, S.A., Moussa, M.E., El-Hadad, S.** Study of Microstructure and Corrosion Behavior of Cast Zn–Al–Mg Alloys *International Journal of Metalcasting* 17 2023: pp. 2794 – 2807. https://doi.org/10.1007/s40962-022-00848-3
10. **Gong, H., Wang, K., Strich, R., Zhou, J.G.** In Vitro Biodegradation Behavior, Mechanical Properties, and Cytotoxicity of Biodegradable Zn–Mg Alloy *Journal of Biomedical Materials Research Part B: Applied Biomaterials* 103 (8) 2015: pp. 1632 – 1640. https://doi.org/10.1002/jbm.b.33353
11. **Moussa, M.E., El-Hadad, S., Shoeib, M.** Influence of Dendritic Fragmentation through Mg Addition on The Electrochemical Characteristics of Zn–0.5 Wt% Al Alloy *International Journal of Metalcasting* 16 (2) 2022: pp. 1034 – 1044. https://doi.org/10.1007/s40962-021-00645-2

12. **Wang, L., Lin, Z., Zhang, Y., Zheng, Y., Han, Y.** Biodegradable Zn–Mg and Zn–Mg–Ca Alloys in Orthopaedic Implants – A Review *Bioactive Materials* 6 (5) 2021: pp. 1665 – 1696. https://doi.org/10.1016/j.bioactmat.2020.11.022
13. **Pieła, K., Błaż, L., Bochniak, W., Ostachowski, P., Łagoda, M., Żabiński, P., Jaskowski, M., Kiper, M., Polkowska, A.** Self-Hardening of Low-Alloyed Zinc for Biodegradable Application *Journal of Alloys and Compounds* 810 2019: pp. 151883. https://doi.org/10.1016/j.jallcom.2019.151883
14. **Du, S., Shen, Y., Zheng, Y., Cheng, Y., Xu, X., Chen, D., Xia, D.** Systematic In Vitro And In Vivo Study on Biodegradable Binary Zn-0.2 At% Rare Earth Alloys (Zn-RE: Sc, Y, La–Nd, Sm–Lu) *Bioactive Materials* 24 2023: pp. 507 – 523. https://doi.org/10.1016/j.bioactmat.2023.04.002
15. **Du, S., Shen, Y., Zheng, Y., Cheng, Y., Xu, X., Chen, D., Xia, D.** Systematic In Vitro and In Vivo Study on Biodegradable Binary Zn-0.2 At% Rare Earth Alloys (Zn-RE: Sc, Y, La–Nd, Sm–Lu) *Bioactive Materials* 24 2023: pp. 507 – 523. https://doi.org/10.1016/j.bioactmat.2023.01.004
16. **Zhao, Q., Liu, Z., Zheng, T., Zhang, L., Li, J., Li, X., Cai, Y.** Substantial Improvement of Mechanical Properties of Zn–Mg Alloys to Orthopedic Implants via Rotary Swaging *Scientific Reports* 15 2025: pp. 29942. https://doi.org/10.1038/s41598-025-15689-z
17. **Dong, C., Liao, Z., Yin, Y., Yi, Y., Zhu, G., Zheng, T., Tan, Q., Xie, Y.** Effects of Nanoscale Precipitates on Mechanical Properties, Corrosion Resistance, and Biocompatibility in Zn–Mn Alloy *Scientific Reports* 15 2025: pp. 5454. https://doi.org/10.1038/s41598-025-89748-w
18. **Tong, X., Miao, D., Zhou, R., Shen, X., Luo, P., Ma, J., Li, Y., Lin, J., Wen, C., Sun, X.** Mechanical Properties, Corrosion Behavior, and In Vitro and In Vivo Biocompatibility of Hot-Extruded Zn-5RE (RE = Y, Ho, And Er) Alloys For Biodegradable Bone-Fixation Applications *Acta Biomaterialia* 185 2024: pp. 55 – 72. https://doi.org/10.1016/j.actbio.2024.07.006